Celal Bayar University Journal of Science

Investigation of Dielectric Anisotropy and Electrical Modulus-Impedance Properties of PCBM/E7 Composite for Organic Electronic Devices Applications

Ahmet Demir[1,2]* , Ahmad Badreddin Musatat[3] , Şule Zeynep Kip[2]

[1] Fibrobeton Inc., İstanbul 34810, Türkiye
[2] Department of Physics, Faculty of Science, Düzce University, Düzce, Türkiye
[3] Department of Chemistry, Faculty of Sciences, Sakarya University, 54050, Sakarya, Türkiye
* ahmetdemir@duzce.edu.tr
* Orcid No: 0000-0002-8702-1941

Abstract

This study investigates the dielectric anisotropy and electrical modulus-impedance properties of a PCBM/E7 composite material for organic electronic devices applications. The research examines a specially fabricated cell combining nematic liquid crystal E7 with [6,6]-phenyl-C61-butyric acid methyl ester (PCBM) semiconductor. Through a comprehensive analysis of dielectric anisotropy, AC conductivity, electrical modulus, and impedance characteristics under varying frequencies and applied voltages (-6.0V to +6.0V), the study reveals distinct behavioral regions and multiple relaxation processes. Key findings include frequency-dependent dielectric anisotropy transitions, enhanced AC conductivity at higher frequencies and voltages, and voltage-modulated impedance characteristics. The observed dual-peak phase angle response suggests multiple relaxation mechanisms, indicating the composite's potential for voltage-tunable electrical properties in advanced optoelectronic applications.

Keywords: AC conductivity, dielectric anisotropy, electrical modulus, impedance spectroscopy, liquid crystal, E7-PCBM composite

1. Introduction

Liquid Crystal (LC)-based materials have gained significant attention due to their numerous electrical and medical uses [1,2]. Also, they occupy a distinct phase between solids and liquids, combining fluid-like properties with solid-like anisotropy. They are primarily categorized into nematic, smectic, and cholesteric phases. In the nematic phase, LC molecules exhibit an average orientational order along their long axes, denoted by the director $\hat{n}$. Nematic LCs are widely employed in display technologies due to their molecular orientation's responsiveness to electric fields. Notably, increasing the applied electric field in nematic LC devices reduces the molecular response time, enhancing performance [3]. This makes nematic LCs versatile for various display sizes, from compact devices (smartphones, calculators, digital cameras) to medium-scale screens (computers) and large displays (projectors, televisions) [4]. On the other hand, Fullerenes, hollow spherical nanoparticles with dimensions similar to LC molecules, serve as ideal dopants for LC hosts. When incorporated into LCs,

fullerenes promote system structurization and self-organization [5]. Pristine fullerene-based LC colloids exhibit enhanced photorefractive effects and photoconductivity [6-8]. Studies have shown that pristine fullerene additives lower the phase transition temperature in nematic LCs with positive dielectric anisotropy, such as E7 and 5CB [9,10]. It is also known that Fullerene additives in nematic LCs reduce the threshold voltage and critical frequency for William's domain formation disappearance, as well as its temporal characteristics [11]. Also doping fullerenes into 90o twisted nematic cells reduces DC driving voltage and improves switching times [12]. A study on the dielectric and electrical properties of an E7 mixture containing methyl Red and fullerene, subjected to AC-DC signals at various temperatures, revealed that both real and imaginary components of dielectric permittivity decreased with increasing frequency of the applied field, while AC conductivity increased [13]. Several investigations on the effect of C60 fullerenes on smectic Liquid crystals exhibited an increase in the transverse component and a decrease in the longitudinal component of the actual dielectric permittivity [14]. The promising properties of

LC materials, especially when doped with fullerenes, open up possibilities for a variety of applications beyond displays. Similarly, Organic Field-Effect Transistors (OFETs) have emerged as important components in modern electronics due to their cost-efficiency and flexibility [15]. LCs, OFETs benefit from advancements in material science and fabrication techniques, which improve their electrical performance and broaden their potential uses. Simultaneously Organic field-effect transistors (OFETs) have gained significant research attention in electronic manufacturing due to their cost-effectiveness and structural flexibility. They find widespread applications in integrated circuits, RFID tags, thin film displays, and sensors, notably employed in organic synthesis to facilitate applications for such field [16-18]. While OFET performance is primarily determined by mobility (μFET), other factors are crucial, like low interfacial resistance between the insulator and gate electrode enhances device efficiency, and the optimal design of the gate-insulator-semiconductor interface is critical to prevent performance-degrading traps [19,20]. While organic field-effect transistors (OFETs) and liquid crystal (LC) devices offer advantages in terms of affordability and performance, research efforts persist in refining their features through the development of new materials and enhanced fabrication processes [21]. In addition, the increasing prevalence of electronic devices has intensified the demand for energy storage and conductive technologies, driving research into sustainable materials. The emergence of flexible electronics, rooted in the 1970s discovery of conductive polymers by Heeger, Shirakawa, and McDiarmid, has revolutionized the field. This advancement allows for the creation of electronic components on various surfaces through the deposition of conductive polymers at multiple scales, facilitating the transformation of industrial byproducts into eco-friendly, high-performance electrical materials [22].

Given the promising properties of liquid crystal materials doped with fullerenes and the growing importance of organic electronic devices, this study aims to revisit and further investigate the dielectric anisotropy and electrical modulus-impedance properties of a novel PCBM/E7 special cell composite medium. Our objectives encompass characterizing the dielectric anisotropy of the PCBM/E7 composite across a range of frequencies and temperatures, as well as analyzing the electrical modulus and impedance properties of this novel composite medium. We also seek to evaluate how the addition of PCBM fullerene derivatives affects the electrical and dielectric properties of the E7 liquid crystal. Furthermore, we aim to explore the potential applications of this PCBM/E7 composite in organic electronic devices, particularly in the context of OFETs and flexible electronics. Through this research, we aim to contribute to the broader understanding of fullerene-doped liquid crystal systems and their potential in next-generation electronic technologies. By investigating the dielectric

anisotropy and electrical modulus-impedance properties of PCBM/E7 special cell as a novel composite medium, we aim to bridge the gap between the theoretical understanding of fullerene-doped liquid crystals and their practical applications in advanced electronic devices.

2. Materials and Methods

2.1. Special Cell Fabrication

A specialized PCBM/E7 composite device with specified contact area of 1.5×10^{-2} cm^2 was fabricated following our previously established protocol [23]. The primary materials, including nematic liquid crystal E7 (a mixture containing 5CB, 7CB, 8OCB, and 5CT compounds) and n-type semiconductor PCBM which chemical structure is given in Figure 1, were sourced from Sigma-Aldrich. E7, characterized by its positive dielectric anisotropy, ($\Delta\varepsilon' \approx$ 13.8 at low frequencies) and broad nematic range (-10°C to 59°C), served as the host material [24,25]. Its unique composition of cyano-biphenyl and terphenyl compounds makes it particularly suitable for optoelectronic applications.

The device fabrication process consisted of several critical steps. Initially, we prepared the semiconductor solution by dissolving PCBM in 1,2-dichlorobenzene to achieve a concentration of 20 mg/mL. This mixture was thoroughly agitated at 60°C for 30 minutes to ensure complete dissolution and homogeneity. For the device structure, we utilized both patterned and unpatterned ITO substrates, serving as source-drain and gate contacts, respectively. The UV-curable NOA65 monomer was selected as the adhesive material for its optimal optical and mechanical properties.
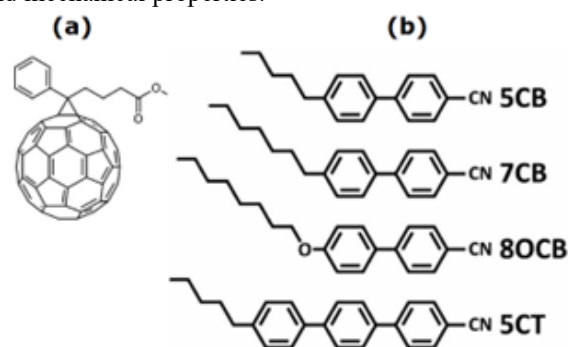
Figure 1. The chemical structure of a) PCBM b) E7 LC.

The OFET cell assembly began with the precise positioning of the ITO substrates, followed by the UV-curing process of NOA65 using 390 nm wavelength radiation. A crucial structural element was the incorporation of a polyimide film spacer (approximately 10 μm thickness), which precisely defined the device's active and insulator layer dimensions. The composite mixture was prepared by combining equal volumes of E7 and the prepared PCBM solution, followed by a 30-minute sonication treatment to achieve uniform

dispersion throughout the medium. The final stage of fabrication involved the careful injection of the PCBM/E7 composite into the prepared cell structure. This process was conducted at an elevated temperature of 120°C, utilizing the capillary filling method. This approach was specifically chosen to minimize exposure to environmental contaminants such as moisture and oxygen, which could potentially compromise device performance. Upon successful filling, the injection ports were thoroughly sealed with epoxy adhesive, ensuring complete isolation from ambient conditions and preventing any potential leakage of the composite material.

2.1.1. Impedance Measurements

The electrical and dielectric properties, polarization, and relaxation mechanisms of the fabricated cell were evaluated using the Keithley 2400 SMU&GW Instek 8105 LCR electrical impedance measurement system, which communicates with a computer via an IEEE 488 card. The entire measurement is shown in scheme 1.


Scheme 1. The conducted impedance measurements.

3. Results and Discussion

Figure 2 presents the frequency-dependent dielectric anisotropy (Δε) which was measured between +6.0 V and 0.0 V of the PCBM/E7 composite by employing equation (1) [26].

$$\Delta_\varepsilon = \varepsilon_{||} - \varepsilon_\perp \tag{1}$$

Were ε_{II} denotes the parallel and $\varepsilon_\perp$ is the perpendicular part of the dielectric constant. The real and imaginary parts of dielectric constant are $\varepsilon'=C/C_0$ and $\varepsilon''=G/\omega C_0$, respectively, here C denoted the capacitance, G/ω illustrated the conductance, and C_0 declares the capacitance of free space. Moreover $C_0=\varepsilon_0 A/d$, ε_0, A, and d were vacuum permittivity ($\varepsilon_0 = 8.85 \times 10^{-14}$ F/cm), active contact area, and thickness of sample, respectively. To determine the dielectric anisotropy value of the PCBM/E7 investigated, the capacitance of the liquid crystal cell was measured as a function of applied voltage. The dielectric anisotropy was calculated as the difference between the permittivities measured parallel and perpendicular to the alignment of the liquid crystal molecules. This parameter is critical in understanding the

orientational ordering and alignment behavior of the liquid crystal molecules in the presence of an external field, which directly impacts the composite's optoelectronic properties. Based on the obtained results at lower frequencies (below approximately 10 kHz), Δε exhibited relatively minor variation, with values remaining negative and close to 5 suggesting that in this frequency range, the dielectric response is predominantly controlled by the relaxation processes associated with the liquid crystal E7, where the orientation of the dipoles does not readily follow the applied field due to the slow response time of the liquid crystals. Meanwhile as the frequency increases beyond 1 kHz, Δε undergoes a marked increase, with a steep rise observed between 1 kHz and 1 MHz. This can be attributed to the onset of a relaxation process, likely the result of reorientation of the liquid crystal molecules aligning with the applied electric field [27]. Interestingly the sharp rise in Δε indicates that the composite material exhibits strong dielectric anisotropy in this frequency range, with the molecular alignment becoming more pronounced. At higher frequencies (above 1 MHz), Δε plateaus, approaching zero. This behavior is typical for dielectric relaxation, where the response of the dipoles in the liquid crystal becomes outpaced by the rapidly alternating electric field. At these frequencies, the dipoles cannot reorient fast enough to contribute to the dielectric anisotropy, and the response becomes frequency-independent. The overall shape of the dielectric anisotropy curve indicated the presence of a clear dielectric relaxation process, which is essential for tuning the composite material's dielectric properties for optoelectronic applications. The observed dielectric anisotropy suggests that the PCBM/E7 composite is well-suited for devices where controlled molecular alignment and dielectric tuning are required, such as in liquid crystal displays (LCDs), photonic devices, and other optoelectronic applications.
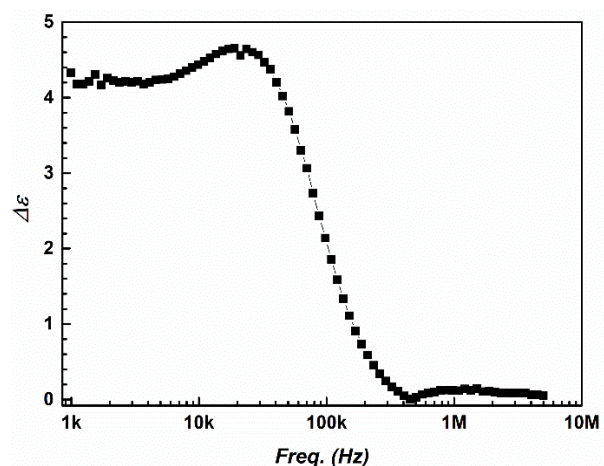
Figure 2. The obtained dielectric anisotropy plot.

On the other hand, in order to gain deeper understanding of critical insights into the conduction mechanisms within the cell, as well as the impact of applied voltage on the material's conductive properties, the AC electrical conductivity (σ_{ac}) of the fabricated special cell as a

function of frequency for different applied DC bias voltages ranging from −6.0 V to 6.0 V was evaluated and illustrated in figure 3. The electrical conductivity was obtained by employing equation (2) as below [28]:

$$\sigma_{ac} = \varepsilon_0 \varepsilon'' \omega \qquad (2)$$

Were σ_{ac} represents the electrical conductivity, and ω represents the angular frequency (2πf). Based on the obtained results at low frequencies (below approximately 10 kHz), σ_{ac} was found to remains relatively constant across all applied voltages, with minimal variation in conductivity. This plateau in conductivity is typical in materials where the conduction mechanism at low frequencies is dominated by localized charge carriers, such as ionic or dipole relaxation processes. The near-zero conductivity in this range suggests that the charge carriers are not sufficiently mobile to contribute to significant AC conductivity at low frequencies, which is common in systems where carrier hopping or dipole orientation under an electric field plays a significant role. As the frequency increases beyond 10 kHz, a sharp rise in conductivity was observed for all voltages. This increase is indicative of a frequency-dependent conductivity mechanism, such as hopping or tunneling of charge carriers between localized states. The observed increase in σ_{ac} as the frequency reaches the MHz range suggests that the charge carriers are gaining sufficient energy to overcome potential barriers, leading to enhanced mobility and higher conductivity [29]. Notably, the applied bias voltage has a clear influence on the AC conductivity, as evidenced by the separation of the conductivity curves at higher frequencies. At higher voltages, particularly at 6.0 V and 4.5 V, the σ_{ac} values at frequencies above 100 kHz were significantly higher compared to those at lower voltages, such as −6.0 V and −4.5 V. This behavior suggests that the applied voltage enhances the mobility of charge carriers of the fabricated special cell, possibly by reducing the potential barriers for conduction or inducing alignment of charge carriers, thereby increasing the overall conductivity.
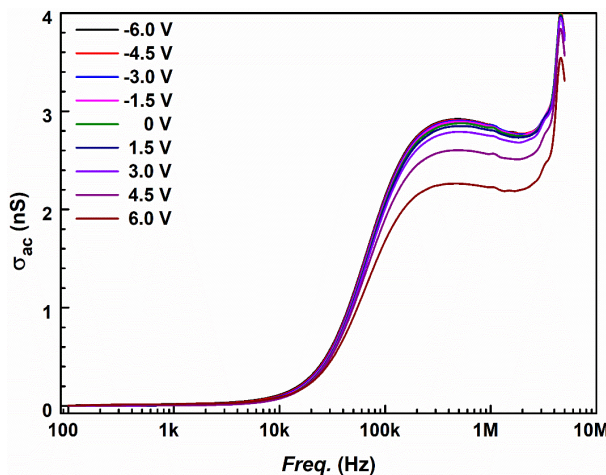

Figure 3. ac electrical conductivity of the fabricated cell

The divergence in σ_{ac} with increasing voltage at higher frequencies highlights the sensitivity of the fabricated device's conductive properties to external electric fields. The increased conductivity at higher voltages is particularly important for applications where tunable electrical properties are desirable, such as in optoelectronic devices, sensors, and capacitive systems. The enhanced conductivity at higher frequencies and voltages suggests that the fabricated special cell can be engineered to operate in high-frequency environments, where rapid charge carrier movement is essential [28].

Figure 4-a presents the frequency dependence of the real part of the electrical modulus (M′) for the fabricated special cell under different applied bias voltages ranging from −6.0 V to 6.0 V by employing equation (3) as below:

$$M'(\omega) = \frac{\varepsilon'}{\varepsilon'^2 + \varepsilon''^2} \quad \text{and} \quad M''(\omega) = \frac{\varepsilon''}{\varepsilon'^2 + \varepsilon''^2} \qquad (3)$$

Were M′, M″ represents the real and the imaginary part of electrical modulus respectively. The real part of the electrical modulus provides insight into the relaxation dynamics and distribution of relaxation times within the material, as well as the degree of conductivity and polarization response of the studied system. At low frequencies (below approximately 10 kHz), M′ were remained relatively constant for all applied voltages, with values ranging from 1000 to 10000. The low values of M′ in this region suggest that the device exhibits significant capacitive behavior, with a high contribution from electrode polarization or space charge effects. This implies that the material has a low electrical modulus, which corresponds to a higher dielectric constant, meaning that the system stores more energy in the form of polarization at lower frequencies. As the frequency increases beyond 10 kHz, M′ showed a gradual increase followed by a distinct peak near 1 MHz for all applied voltages. This rise in M′ with frequency reflected the onset of dielectric relaxation, where the dipoles or charge carriers begin to respond to the applied AC field but with increasing difficulty as the frequency becomes higher. The appearance of a peak in M′ around 1 MHz is characteristic of the device's dielectric relaxation process, where the bulk polarization of the material starts to lag behind the rapidly changing field, resulting in a reduction of the material's ability to store charge. Notably, at higher frequencies (above 1 MHz), M′ shows a significant spike for all voltages, with the magnitude of the modulus increasing with the applied voltage. This behavior indicates that the relaxation time of the charge carriers shortens at higher frequencies, leading to an increased response in the real part of the modulus. The higher M′ values at elevated frequencies suggest that the material becomes more conductive and less capable of storing charge, as the applied AC field is too rapid for significant polarization to occur. The effect of the applied voltage is apparent in the divergence of the modulus curves at higher frequencies. Higher applied voltages,

A. Demir

particularly 6.0 V and 4.5 V, lead to a more pronounced increase in M′, suggesting that the external field enhances the relaxation process and the movement of charge carriers. which indicates that the relaxation dynamics and conductivity of the material are sensitive to the applied voltage, with higher voltages inducing more rapid polarization and charge carrier mobility. On the other hand, figure 4-b presents the frequency dependence of the imaginary part of the electrical modulus (M″) for the fabricated special cell under varying applied voltages, ranging from −6.0 V to 6.0V. The imaginary part of the modulus is closely related to the energy dissipation within the material and reflects the degree of relaxation of the polarization processes in the system. Based on the obtained results, at low frequencies (below approximately 10 kHz), M″ exhibits relatively low values for all applied voltages, typically under 1,000. This region indicates that at low frequencies, the material displays minimal relaxation and dissipative effects. The polarization aligns relatively easily with the applied field, and the stored energy is primarily in the form of reversible polarization, with little energy loss due to dielectric relaxation. As the frequency increases beyond 10 kHz, M″ shows a clear increase, eventually reaching a broad peak around 1 MHz for all voltages. This peak represents the relaxation process, where the dipoles in the material can no longer follow the rapidly changing electric field, leading to energy dissipation. The presence of this peak is characteristic of dielectric materials that exhibit a relaxation time, and the frequency at which this peak occurs provides information on the relaxation dynamics of the system. The effect of the applied voltage is particularly evident in the lower frequency region, where the magnitude of M″ diverges for different voltages. Higher voltages, such as −6.0 V and 6.0 V, result in slightly larger values of M″, suggesting that increasing the applied voltage enhances the polarization response and energy dissipation within the material. This indicates that the polarization dynamics are sensitive to the external electric field, with higher fields inducing more significant dielectric relaxation effects. At high frequencies (beyond 1 MHz), the modulus decreases sharply, indicating that the dipoles or charge carriers are unable to respond to the fast-alternating field. In this region, M″ reaches a plateau, where the material transitions to a purely conductive state with minimal energy storage or dissipation in the form of polarization. This high-frequency behavior is typical of materials that exhibit conductive loss rather than dielectric relaxation at very high frequencies. The imaginary modulus curves for different voltages converge at high frequencies, suggesting that the relaxation dynamics are largely voltage-independent in this regime. This implies that while the applied field influences the polarization and relaxation behavior at lower frequencies, at higher frequencies, the system behaves in a more uniform manner across the voltage range. The physical mechanism by which electrical charge conduction within the cell is depicted is given in Figure 5.
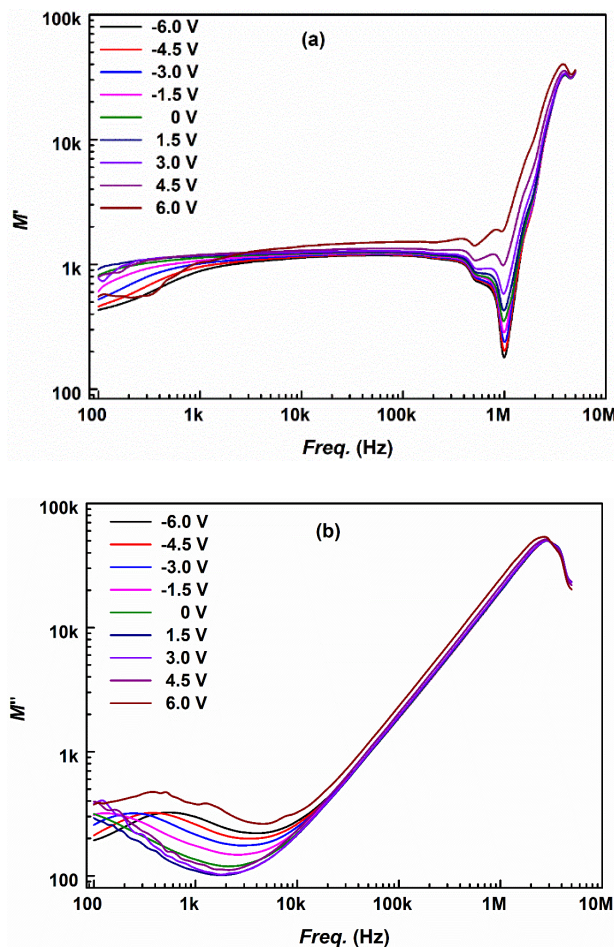

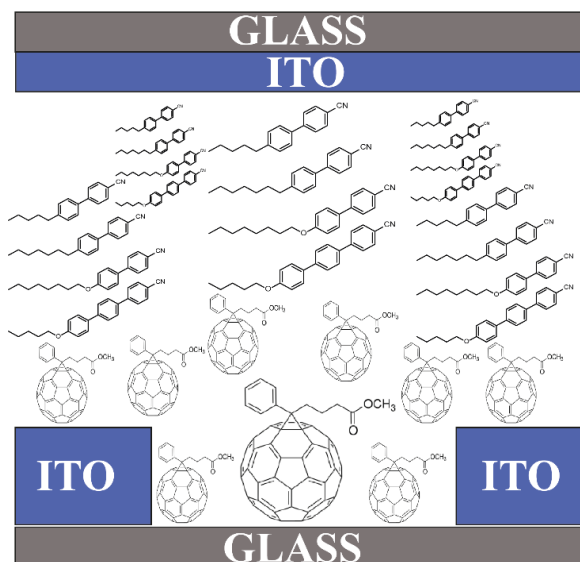**Figure 4.** a) the real b) imaginary part of the electrical modulus of fabricated cell.

Figure 5. Real time electrical charge transfer mechanism of the fabricated cell.

Figure 6-a. shows the variation of the real part of impedance (Z') versus frequency for the fabricated device under different applied gate voltages (V $_{GS}$) ranging from -6.0 V to +6.0 V by employing equation (4):

$$Z' = \frac{\varepsilon''}{\omega C_o \left[\varepsilon'^2 + \varepsilon''^2\right]} \text{ and } Z'' = \frac{\varepsilon'}{\omega C_0 \left[\varepsilon'^2 + \varepsilon''^2\right]} \qquad (4)$$

Where Z', Z'' represents the real and imaginary part of impedance which after all can be obtained from the ε' and ε'' values for each frequency. Based on the obtained results, the impedance spectrum exhibited three distinct regions: Low-frequency region (100 Hz - 10 kHz): Z' decreases rapidly with increasing frequency, indicating a strong frequency dependence of the device's resistive behavior. Mid-frequency region (10 kHz - 1 MHz): Z' plateaus, suggesting a relatively stable resistive component in this frequency range. High-frequency region (> 1 MHz): A sharp drop in Z' was observed, likely due to the device's capacitive effects becoming dominant. The applied gate voltage influences the impedance response, particularly in the low-frequency region, where higher positive and negative V_{GS} values result in slightly increased Z'. This behavior suggests that the gate voltage modulates the charge transport mechanisms within the device, affecting its overall impedance characteristics. The observed trends provide valuable insights into the frequency-dependent electrical properties of the fabricated device and the impact of gate voltage on charge dynamics within the device structure. Meanwhile figure 6-b illustrates the frequency dependence of the imaginary part of impedance (Z'') for the special cell at various gate voltages (V_{GS}) from -6.0 V to +6.0 V was found to reveal several key features: Low-frequency region (100 Hz - 10 kHz): Z'' decreases linearly with increasing frequency, indicating a dominant capacitive behavior. For the Mid-frequency region (10 kHz - 100 kHz): A minimum in Z'' was observed, suggesting a transition in the device's electrical response. Lastly, under the High-frequency region (100 kHz - 10 MHz): A prominent relaxation peak appears, with its maximum around 1-2 MHz. This peak signifies a relaxation process, likely associated with interfacial polarization or charge carrier dynamics within the device. The applied gate voltage influences the relaxation peak intensity, with higher positive V_{GS} values resulting in lower peak magnitudes. This voltage dependence implies that the gate bias modulates the relaxation processes, possibly by altering the charge distribution or molecular alignment in the LC-PCBM composite. The observed Z'' spectrum provided valuable insights into the capacitive nature and relaxation mechanisms of the LC- PCBM composite cell, complementing the real impedance data and offering a more complete picture of the device's complex electrical behavior.
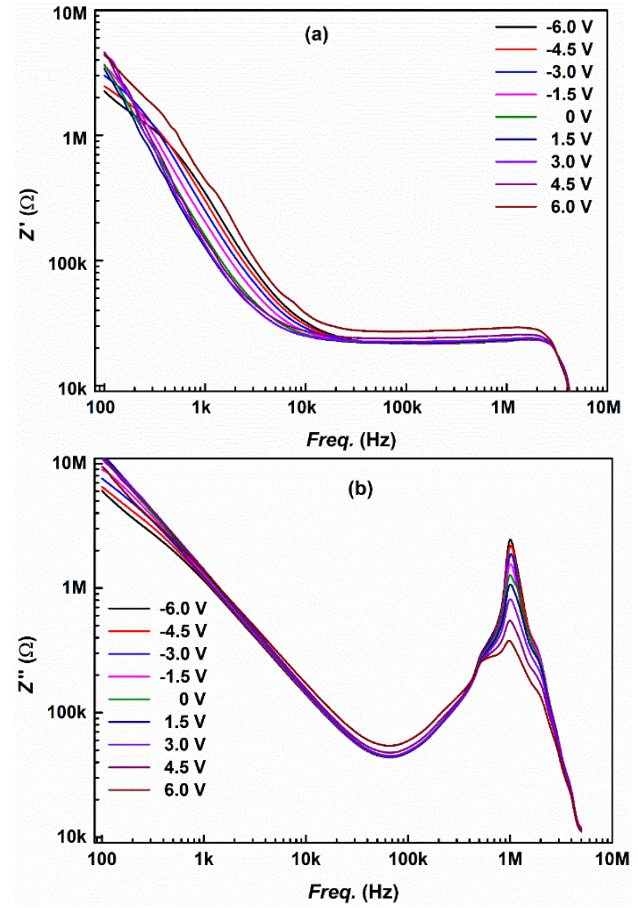
Figure 6. a) The variation of real part b) imaginary part of impedance versus frequency of fabricated cell

Figure 7 illustrates the phase angle's frequency dependence for the LC-PCBM special cell under various gate voltages (V_{GS}) from -6.0 V to +6.0 V by employing the equation (5):

$$tan\theta = \frac{Z''}{Z'} \qquad (5)$$

The spectrum reveals intricate electrical behavior with multiple relaxation processes: In the low-frequency domain (100 Hz - 10 kHz), the phase angle rises with frequency, peaking around 5-10 kHz, indicating a shift from resistive to capacitive characteristics. The mid-frequency range (10 kHz - 100 kHz) shows a sharp phase angle decline, suggesting a return to more resistive behavior. At high frequencies (100 kHz - 10 MHz), a second, more prominent maximum emerges near 1 MHz before rapidly decreasing, likely signifying a distinct relaxation process within the device. The applied gate voltage markedly affects the phase angle response, especially in low and high-frequency regions. As V_{GS} shifts from negative to positive, the first phase angle peak (5-10 kHz) diminishes, while the second peak (1 MHz) remains relatively stable. This voltage-dependent behavior suggests that gate bias modulates the device's resistive and capacitive components, possibly through altering charge carrier dynamics or LC-PCBM composite molecular arrangement. The observation of two distinct

phase angle maxima indicates multiple relaxation mechanisms at different timescales. These may stem from interfacial polarization, charge trapping/detrapping, or molecular reorientation within the liquid crystal matrix. These insights into the LC-PCBM's complex impedance characteristics highlight its potential for gate voltage-tunable electrical properties.
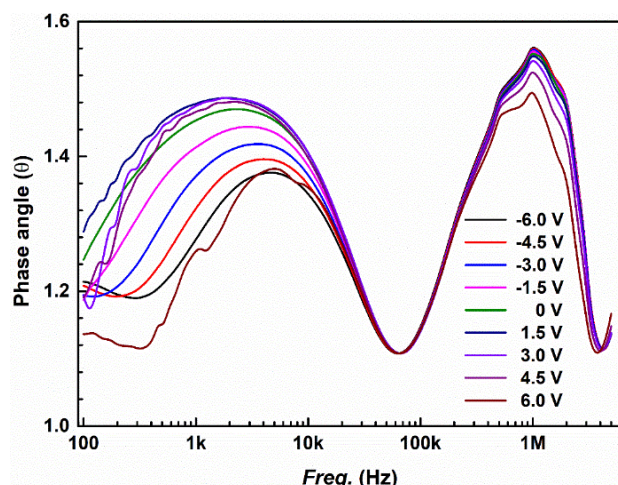
Figure 7. Phase angle of the fabricated special cell

Conclusion

In this study, we have thoroughly investigated the dielectric anisotropy and electrical modulus-impedance properties of a PCBM/E7 composite medium for enhanced optoelectronic applications. The dielectric anisotropy measurements revealed that at lower frequencies (below 10 kHz), $\Delta\varepsilon$ exhibited relatively minor variation, with values remaining negative and close to -5×10^{-5}. A marked increase in $\Delta\varepsilon$ was observed between 10 kHz and 1 MHz, followed by a plateau approaching zero at higher frequencies, indicating well-defined dielectric relaxation processes. The AC conductivity analysis demonstrated frequency and voltage-dependent behavior, with significant enhancement at frequencies above 100 kHz, particularly at higher applied voltages (6.0 V and 4.5 V). The electrical modulus studies showed distinct relaxation dynamics, with the real part (M') exhibiting a characteristic peak near 1 MHz and significant voltage dependence at higher frequencies. The imaginary part (M'') revealed a broad relaxation peak around 1 MHz, indicating complex polarization processes within the material. Impedance spectroscopy identified three distinct frequency regions in Z' and Z'', with multiple relaxation processes evidenced by dual-phase angle maxima at 5-10 kHz and 1 MHz. The findings show that PCBM/E7 composite exhibits complex charge transport and voltage-tunable properties, making it a promising candidate for advanced optoelectronic applications. The observed voltage-dependent behavior and multiple relaxation processes suggest potential applications in display technologies and electronic devices where precise control of electrical properties is essential.

Ethics

There are no ethical issues after the publication of this manuscript.

References

[1]. Judele, R., Laschat, S., Baro, A., Nimtz, M. 2006. Gallic esters of 4,5-dinitrocatechol as potential building blocks for thermotropic liquid crystals. Tetrahedron; 62(41): 9681–9687.

[2]. Chavda, V.P., Shah, K.N., Soni, S., Tripathi, M., Bhargava, S., Thakur, M., Parikh, P., Vora, L.K., Thakor, P., Makwana, M., Kapadia, N. 2023. Lyotropic liquid crystalline phases: Drug delivery and biomedical applications. International Journal of Pharmaceutics; 647: 123546.

[3]. Takikawa, Y., Kaneko, K., Odani, S., Ikemura, T., Iwata, M. 2020. Dielectric anisotropy in PCPB/MBBA mixtures showing the dual frequency characteristic. Japanese Journal of Applied Physics; 59(SD): SDDB05.

[4]. Sasani Ghamsari, M., Carlescu, I. (Eds.). 2020. Liquid Crystals and Display Technology. IntechOpen.

[5]. Kamanina, N.V., Serov, S.V., Savinov, V.P., Uskoković, D.P. 2005. Self-organization and dynamic characteristics study of nanostructured liquid crystal compounds. Solid State Phenomena; 106: 145–148.

[6]. Khoo, I.C., Chen, C.W., Ho, T.J. 2016. Observation of photorefractive effects in blue-phase liquid crystal containing fullerene-C_{60}. Optics Letters; 41(1): 123.

[7]. Kamanina, N.V., Serov, S.V., Savinov, V.P., Uskoković, D.P. 2010. Photorefractive and photoconductive features of the nanostructured materials. International Journal of Modern Physics B; 24(06n07): 695–702.

[8]. Zhang, Y., Yao, F., Pei, Y., Sun, X. 2009. High-diffraction-efficiency holographic gratings in C60-doped nematics. Applied Optics; 48(33): 6506–6510.

[9]. Okutan, M., San, S.E., Basaran, E., Yakuphanoglu, F. 2005. Determination of phase transition from nematic to isotropic state in carbon nano-balls doped nematic liquid crystals by electrical conductivity-dielectric measurements. Physics Letters A; 339(6): 461–465.

[10]. Ibragimov, T.D. 2021. Effect of fullerenes C60 on dielectric relaxation, electric conductivity, and electro-optic properties of 4-cyano-4′-pentylbiphenyl. Fullerenes, Nanotubes and Carbon Nanostructures; 29(6): 457–463.

[11]. Ibragimov, T.D. 2021. Influence of fullerenes C60 and single-walled carbon nanotubes on the Carr–Helfrich effect in nematic liquid crystal. Optik; 237: 166768.

[12]. Lee, W., Wang, C.Y., Shih, Y.C. 2004. Effects of carbon nanosolids on the electro-optical properties of a twisted nematic liquid-crystal host. Applied Physics Letters; 85(4): 513–515.

[13]. Okutan, M., San, S.E., Köysal, O., Şentürk, E. 2010. The electrical properties of a fullerene and C.I. Acid Red 2 (methyl red) doped E7 nematic liquid crystal. Dyes and Pigments; 84(3): 209–212.

[14]. Ibragimov, T.D., Imamaliyev, A.R., Ganizade, G.F. 2020. The threshold voltage, dielectric and conductivity properties of C60-doped smectic A liquid crystal. Fullerenes, Nanotubes and Carbon Nanostructures; 28(6): 509–514.

[15]. Demir, A., Musatat, A.B. 2024. Evaluation of industrial Poly(tert-butyl acrylate) insulated A p-channel organic field-effect transistor (PtBA-p-OFET). Düzce Üniversitesi Bilim ve Teknoloji Dergisi; 12(3): 1762–1770.

[16]. Sheraw, C.D., Zhou, L., Huang, J.R., Gleskova, H., Wagner, S., Jackson, T.N. 2002. Organic thin-film transistor-driven polymer-dispersed liquid crystal displays on flexible polymeric substrates. Applied Physics Letters; 80(6): 1088–1090.

[17]. Rogers, J.A., Bao, Z., Makhija, A., Feng, Y., Zhang, Y., Mahajan, A., Veroff, R., Jones, T., MacLean, J., Schlittler, R., Whitesides, G.M. 2001. Paper-like electronic displays: Large-area rubber-stamped plastic sheets of electronics and microencapsulated electrophoretic inks. Proceedings of the National Academy of Sciences; 98(9): 4835–4840.

[18]. Musatat, A.B., Atahan, A., Aksu, M., Zengin, M. 2022. Employing of 2-Acetylpyridine based chalcone as Hg^{2+} sensing material: Experimental and theoretical examination. Düzce University Journal of Science and Technology Research; 10(4): 2133–2143.

[19]. Mas-Torrent, M., Rovira, C. 2011. Role of molecular order and solid-state structure in organic field-effect transistors. Chemical Reviews; 111(8): 4833–4856.

[20]. Walser, M.P., Kalb, W.L., Mathis, T., Batlogg, B. 2009. Low-voltage organic transistors and inverters with ultrathin fluoropolymer gate dielectric. Applied Physics Letters; 95(23): 233301.

[21]. Fang, X., Wei, Z., Qi, L., Chen, J., Wang, C., Ge, L., Yan, F. 2021. Patterning liquid crystalline organic semiconductors via inkjet printing for high-performance transistor arrays and circuits. Advanced Functional Materials; 31(21): 2100237.

[22]. Gencel, O., Musatat, A.B., Demir, A., Tozluoğlu, A., Tutuş, A., Kıllı, A., Fidan, H., Çavuş, K.F. Transforming industrial byproduct to eco-friendly functional material: Ground-granulated blast furnace slag reinforced paper for renewable energy storage. Science of the Total Environment; 176616.

[23]. Kip, Ş., Gegin, K., Demir, A., Köysal, O., Öztürk, S., Kösemen, A. 2023. The novel n-channel liquid crystal organic field effect transistor (LC-n-OFET): A promising technology for low-power electronics. Organic Electronics; 106965.

[24]. Katariya-Jain, A., Deshmukh, R.R. 2022. Effects of dye doping on electro-optical, thermo-electro-optical, and dielectric properties of polymer dispersed liquid crystal films. Journal of Physics and Chemistry of Solids; 160: 110363.

[25]. Mi, X.D., Yang, D.K. 1998. Capillary filling of nematic liquid crystals. Physical Review E; 58(2): 1992–2000.

[26]. Lueder, E. 2010. Liquid Crystal Displays: Addressing Schemes and Electro-Optical Effects. Wiley.

[27]. Kocakülah, G. 2023. The role of rubrene concentration on dielectric parameters of nematic liquid crystal. Hittite Journal of Science and Engineering; 10(3): 193–199.

[28]. Subaşı, A., Emiroğlu, M., Demir, A. 2023. Polarization and relaxation mechanisms in glass fiber-reinforced LED-cured polyester composites incorporating graphene nanotubes. Materials Science and Engineering B; 295: 116614.

[29]. Demir, A., Köysal, O. 2016. Investigation of photo-induced change of electro-optical performance in a liquid crystal-organic field effect transistor (LC-OFET). Philosophical Magazine; 96(22): 2362–2371.